# Core−Shell Microspherical $Ti_{1-x}Zr_xO_2$ Solid Solution Photocatalysts Directly from Ultrasonic Spray Pyrolysis

**Yu Huang,[†] Zhi Zheng,[‡] Zhihui Ai,[†] Lizhi Zhang,*[,†] Xiaoxing Fan,[§] and Zhigang Zou[§]**

*Key Laboratory of Pesticide & Chemical Biology of Ministry of Education, College of Chemistry, Central China Normal University, Wuhan 430079, P. R. China, Institute of Surface Micro and Nano Materials, Xuchang University, Xuchang 461000, P. R. China, and Ecomaterials and Renewable Energy Research Center (ERERC), Department of Physics, Nanjing University, Nanjing 210093, P. R. China*

*Received: July 2, 2006; In Final Form: August 7, 2006*

A series of $Ti_{1-x}Zr_xO_2$ solid solutions photocatalysts ($x = 0.000$, 0.045, 0.090, 0.135, and 0.180) was directly obtained by an ultrasonic spray pyrolysis method. Compared with previous methods for solid solutions, our preparation was very fast. The resulting samples were characterized by X-ray diffraction, scanning electron microscopy, transmission electron microscopy, high-resolution transmission electron microscopy, nitrogen adsorption, and UV−vis diffuse reflectance spectroscopy. The characterizations revealed core−shell spherical structures of the resulting solid solutions. We evaluated photocatalytic activities of the solid solutions on degradation of rhodamine B in aqueous solution under simulated solar light. It was found that $Ti_{0.91}Zr_{0.09}O_2$ solid solution exhibited the highest photocatalytic activity among all the as-prepared samples. Its activity was much higher than that of P25. The formation mechanism of core−shell spherical structures was proposed. Moreover, we successfully extended this method to prepare microspheres of ceria and ceria−zirconia solid solutions. We think this general method may be easily scaled up for industrial production of microspherical solid solutions photocatalysts and catalysts.

## 1. Introduction

Semiconductor heterogeneous photocatalysis has attracted much attention because of its application to the decomposition of undesirable chemical contaminants in water and air.[1−5] Titania has been intensively studied for its versatility in optical, electrical, and photochemical properties, and thus it has been applied in high-refractive optics, oxide semiconductors, oxygen sensors, photovoltaics, photocatalysts, and so on.[6−14] Anatase-type $TiO_2$, which shows the highest photocatalytic performances among the three different crystalline forms, has been widely utilized for photocatalytic decomposition of harmful organic components. Recently, titania-based photocatalysts were also applied to remove atmospheric $NO_x$, which is believed to cause acid rain and to be toxic to human health.[15] The reasons for this choice are its high photostability, nontoxicity, low cost, and availability.[16] To enhance the quantum efficiency of $TiO_2$, many efforts have been made to improve the intrinsic efficiency of $TiO_2$. These include doping by transition metals, nonmetal atoms, sensitization, application of composite semiconductors, and addition of noble metals.[17−21]

In 1997, Yu and co-workers discovered that solid solutions with the composition of $Ti_{1-x}V_xO_2$ were effective photocatalysts for the degradation of acetone.[22] Following this pioneering work, $Ti_{1-x}Zr_xO_2$ solid solutions ($x = 0.000$, 0.025, 0.050, 0.075, and 0.100) were successfully prepared by a citric acid complexing method with $ZrCl_4$ and $TiCl_4$ as precursors. When $Ti^{4+}$ ions in titania lattice were partially substituted with $Zr^{4+}$ to form $Ti_{1-x}Zr_xO_2$ solid solutions, the resulting solid solutions showed enhanced photocatalytic activities on the oxidation of acetone.[23] However, their preparation required multiple steps, including aging of 24 h and thermal posttreatment of 5 h. Therefore, it is still a challenge to develop a simple and time-saving approach to produce solid solutions with high photocatalytic activity, especially for industrial scaling up.

Solid solutions were also reported to be prepared by using sol−gel, coprecipitation, solid-state reaction, and sonochemical synthesis.[24−30] In comparison with these methods, aerosol-assisted methods are scalable. They have been widely used for the synthesis of a variety of inorganic and organic materials, such as porous inorganic oxide nanomaterials and silica-encapsulated metal nanoparticles.[31−33] Among aerosol-assisted methods, ultrasonic spray pyrolysis (USP) is often used to prepare fine-grained powders.[34−36] In USP, the precursor solution was first nebulized by commercial ultrasonic nebulizer; the resulting droplets were then transported by the carrier gases to a heated furnace tube, where several reactions, such as solvent evaporation and atomic rearrangement, take place in a continuous flow process. Particle size, phase purity, and morphology can be easily controlled during the process. Therefore, it is very simple in comparison with other methods.[37] For instance, Suslick and co-workers utilized ultrasonic spray pyrolysis (or aerosol-assisted methods) to prepare magnetic and porous $SiO_2$ nanosphere, high surface area $MoS_2$ very recently.[32,38]

To the best of our knowledge, there is no report about the synthesis of solid solutions with USP. Herein we report that $Ti_{1-x}Zr_xO_2$ solid solutions can be obtained in one step via an ultrasonic spray pyrolysis method. The as-prepared solid solutions were microspheres with core−shell structures and exhibited high photocatalytic activity on the degradation of rhodamine B (RhB) in aqueous solution. Moreover, we successfully extended

* Address correspondence to this author. E-mail: zhanglz@mail.ccnu.edu.cn. Tel/fax: +86-27-6786 7535.
[†] Central China Normal University.
[‡] Xuchang University.
[§] Nanjing University.

10.1021/jp064135o CCC: $33.50 
Published on Web 09/14/2006

our method to prepare microspheres of ceria and ceria−zirconia solid solutions, indicating its generality.

## 2. Experimental Section

**2.1. Synthesis of $Ti_{1-x}Zr_xO_2$ Solid Solutions.** $Ti_{1-x}Zr_xO_2$ solid solutions ($x = 0.000$, 0.045, 0.090, 0.135, and 0.180) were prepared by an ultrasonic spray pyrolysis method. $TiCl_4$ and $ZrOCl_2 \cdot 8H_2O$ with required stoichiometry were added to 60 mL of distilled water at 4 °C under vigorous stirring. The solutions were nebulized using an ultrasonic nebulizer at 1.7 MHz ± 10% (YUYUE402AI, Shanghai) and then carried by a nitrogen flow though a quartz tube surrounded by a furnace thermostated at 600 °C for 1 h, in which the flow rate of the nitrogen gas was controlled at 43 $L \cdot h^{-1}$. The quartz reaction tube with the diameter of 3.5 cm was 1 m long. The products were collected in a percolator with distilled water and then filtered by a fritted glass funnel, washed thoroughly with distilled water and ethanol, and finally dried in an oven at 50 °C. The whole apparatus was similar to that reported by Didenko and Suslick.[39]

**2.2. Characterization.** The powder X-ray diffraction (XRD) patterns were recorded on a Rigaku D/MAX-RB diffractometer with monochromatized Cu Kα radiation ($\lambda = 1.5418$).

Scanning electron microscopy (SEM, JSM-5600) was used to characterize the morphology of the solid solutions.

Transmission electron microscopy (TEM) study was carried out on a Philips CM-120 electron microscopy instrument. The samples for TEM were prepared by dispersing the final powders in ethanol; the dispersion was then dropped on carbon−copper grids.

The nitrogen adsorption and desorption isotherms at 77 K were measured using a Micrometritics ASAP2010 system after samples were vacuum-dried at 473 K overnight.

A Varian Cary 100 Scan UV−visible system equipped with a labsphere diffuse reflectance accessory was used to obtain the reflectance spectra of the catalysts over a range of 200−600 nm. Labsphere USRS-99-010 was employed as a reflectance standard.

X-ray photoelectron spectroscopy (XPS) measurements were performed in a VG Scientific ESCALAB Mark II spectrometer equipped with two ultrahigh-vacuum (UHV) chambers. All the binding energies were calibrated to the C 1s peak at 284.8 eV of the surface adventitious carbon.

**2.3. Photocatalytic Activity Test.** The photocatalytic activities of the samples were evaluated on the degradation of RhB in an aqueous solution under simulated solar light from a 500-W tungsten halogen lamp without cutoff filter. The lamp was set inside a cylindrical vessel surrounded by a circulating water jacket for cooling. A 0.1 g amount of photocatalyst was added into 100 mL of 5 $mg \cdot L^{-1}$ RhB aqueous solution in a container with cooling water jacket outside. The temperature of the solution during the photodegradation was kept at about 25 °C. The RhB solution with photocatalyst was continuously stirred for 1 h to ensure the establishment of an adsorption−desorption equilibrium among the photocatalyst, RhB, and water before the lamp was turned on. The lamp was placed under the bottom of the RhB solution with about 15 cm in distance. During the degradation, the RhB solution with photocatalyst was continuously stirred by a dynamoelectric stirrer and the concentration of RhB was monitored by colorimetry with a U-3310 UV−vis spectrometer (Hitachi).

## 3. Results and Discussion

**3.1. XRD Patterns.** The X-ray diffraction was used to characterize the phase structure of the products. Figure 1 shows

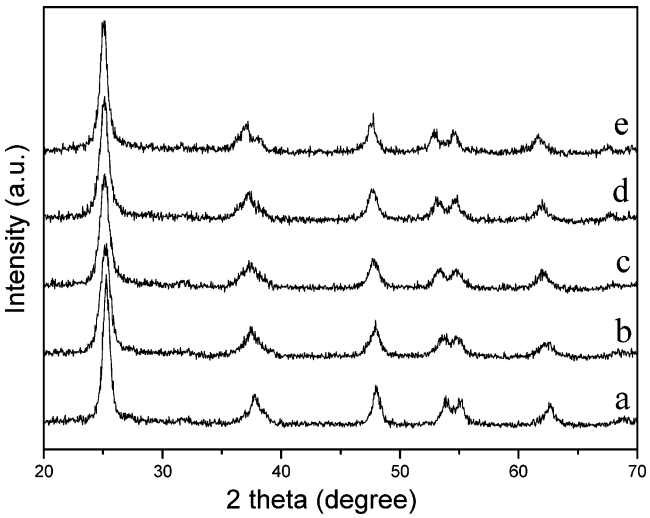


**Figure 1.** XRD patterns of the as-prepared $Ti_{1-x}Zr_xO_2$ samples: (a) $x = 0.000$; (b) $x = 0.045$; (c) $x = 0.090$; (d) $x = 0.135$; (e) $x = 0.180$.

powder XRD patterns of the as-prepared samples. It was found that anatase (JCPDS, file No. 21-1272) existed in all the as-prepared samples. With an increase in zirconium content, the XRD peaks gradually shift to lower diffraction angles, revealing the formation of titania−zirconia solid solutions. As the larger $Zr^{4+}$ replaces $Ti^{4+}$ in anatase $TiO_2$, the lattice parameter would increase.[25] The crystal sizes of the solid solution estimated from the (101) peaks were 12.2, 8.4, 9.0, 9.3, and 11.5 nm for the $Ti_{1-x}Zr_xO_2$ samples ($x = 0.000$, 0.045, 0.090, 0.135, and 0.180), respectively. Therefore, in comparison with the undoped $TiO_2$ sample, the introduction of zirconium inhibited the crystalline grain growth of the solid solutions by providing dissimilar boundaries,[23,24] although the crystal sizes of solid solutions grew gradually larger with increasing zirconium contents.

**3.2. SEM Images.** Figure 2 shows SEM images of the as-prepared $Ti_{1-x}Zr_xO_2$ samples. It was found that spherical particles were obtained in all the samples. The sizes of these spheres were not uniform. Their diameters were in the range of several hundred nanometers to several micrometers. With an increase in zirconium content, the microstructures of the solid solution spheres changed slightly. Some core−shell structured spheres could be observed in pure $TiO_2$ without zirconium substitution (Figure 2a). Core−shell structured spheres were also observed in the $Ti_{0.955}Zr_{0.045}O_2$ solid solution. The surface of the shell were smooth, but the inner core was very rough (Figure 2b). The thicknesses of the shell were about 200 nm. When the content of zirconium increased to 0.090, the core−shell structures in the $Ti_{0.910}Zr_{0.090}O_2$ solid solution became those consisting of small spheres (core) enwrapped in big spherical containers (shell) with about 500 nm in thickness (Figure 2c). The small spheres were 300−400 nm in diameters. With an increase in the content of zirconium to 0.135, the core−shell structures further changed. We observed many hollow semispheres with about 2 μm in diameter and smaller spheres with about 500 nm in diameters (Figure 2d). Those smaller spheres were believed to be released from the hollow semispheres. This thought was confirmed by the SEM image of the solid solution with highest zirconium content (Figure 2e), in which we observed some broken hollow spheres with many small spheres enwrapped.

**3.3. TEM Images.** The resulting $Ti_{1-x}Zr_xO_2$ nanostructures were further investigated by transition electron microscopy. Figure 3 shows representative TEM images of the as-prepared $Ti_{1-x}Zr_xO_2$ samples. In Figure 3a the contrast between gray edge

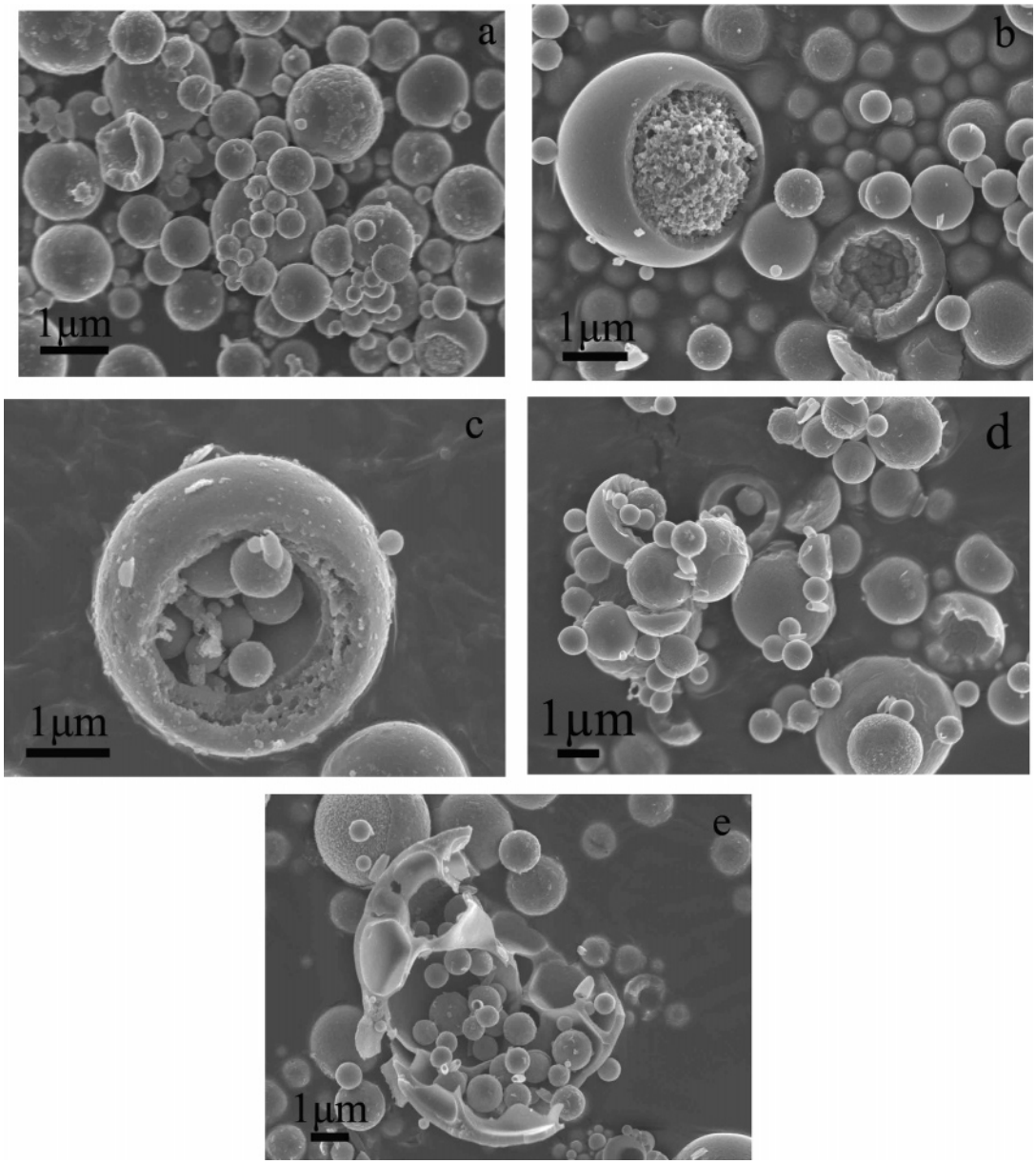


**Figure 2.** SEM images of the as-prepared $Ti_{1-x}Zr_xO_2$ samples: (a) $x = 0.000$; (b) $x = 0.045$; (c) $x = 0.090$; (d) $x = 0.135$; (e) $x = 0.180$.

and dark center of the spheres is clearly observed, confirming the core−shell structure of $Ti_{0.910}Zr_{0.090}O_2$. The sizes of the spheres in Figure 2a were about 500 nm in diameter. In Figure 2b, we observe not only the contrast between gray edge and dark center of the spheres but also some shells peeled off from the spheres by sonication during the preparation of TEM sample. It is interesting to find a complex core−shell structure in the TEM image of the $Ti_{0.820}Zr_{0.180}O_2$ solid solution (Figure 3c). We observe six chambers in a sphere with about 4 $\mu$m in diameter. Small spheres with diameters of 150−800 nm were located in the chambers of the big sphere. This observation confirms the SEM results. Moreover, mesopores could be observed in the shell of the big hollow sphere in Figure 3c.

**3.4. UV−Vis Diffuse Reflectance Spectra.** Figure 4 displays UV−vis diffuse reflectance spectra of the as-prepared $Ti_{1-x}Zr_xO_2$ samples (inset). Assuming the solid solutions to be indirect semiconductor, as is $TiO_2$, plots of the $(ah\nu)^{1/2}$ versus the energy of absorbed light afford the band gaps of solid solutions as shown in Figure 4. The band gaps optically obtained in such a way were approximately 2.88, 2.92, 2.94, 3.00, and 3.03 eV for the $Ti_{1-x}Zr_xO_2$ samples ($x = 0.000$, 0.045, 0.090, 0.135, and 0.180), respectively. Therefore, we conclude that the introduction of zirconium can enlarge the band gap of $TiO_2$.

**3.5. Nitrogen Sorption.** The porous structures of the resulting samples were studied by nitrogen sorption. Figure 5 presents the nitrogen adsorption−desorption isotherms and Barret−Joyner−Halenda (BJH) pore size distribution curve (inset) of the $Ti_{0.820}Zr_{0.180}O_2$ solid solution (other isotherms were in the Supporting Information). Figure 5 displays type IV adsorption−desorption isotherms, which is caused by the weak interaction of adsorbent−adsorbent and the existence of porous structures in the sample. A hysteresis loop, which is commonly associated with the presence of mesoporosity, is a common feature of type IV isotherms. Capillary condensation gives rise to the hysteresis loop. In the nitrogen adsorption−desorption isotherms, there are hysteresis loops at $0.41 < P/P_0 < 0.95$ in the isotherms of all the samples, corresponding to the filling of mesopores produced by the agglomeration of primary particles in the spheres.[41] These results are consistent with the observation in TEM image (Figure 3c). The Brunauer−Emmett−Teller (BET) specific surface areas, pore volumes, and mean pore diameters of the $Ti_{1-x}Zr_xO_2$ samples are summarized in Table 1. It was

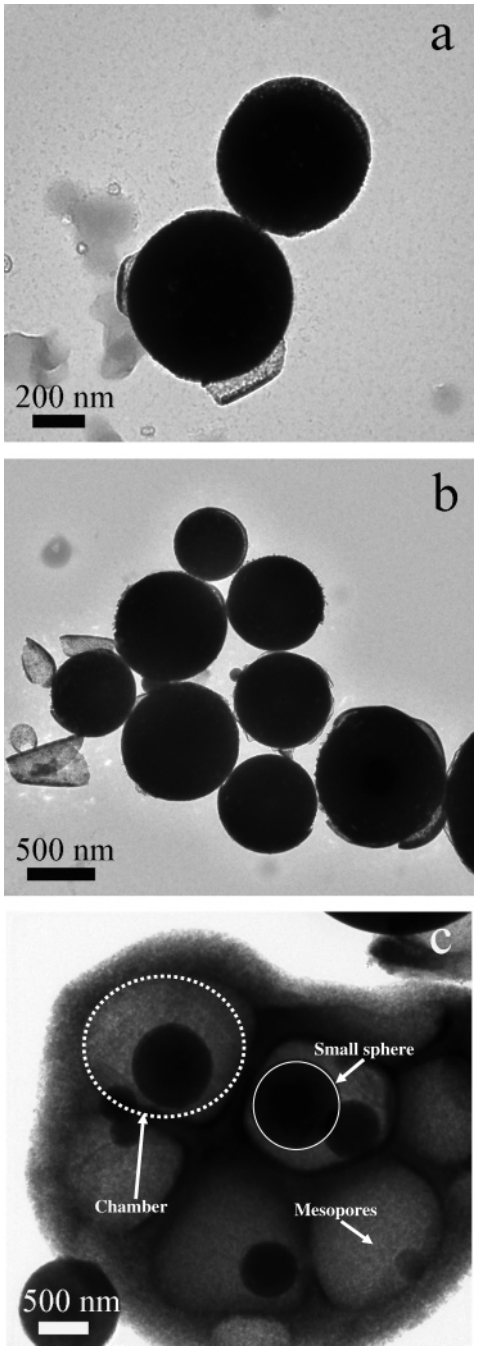


**Figure 3.** TEM images of the as-prepared $Ti_{1-x}Zr_xO_2$ solid solutions: (a) $x = 0.090$; (b) $x = 0.135$; (c) $x = 0.180$.

found that surface areas of the solid solutions increased with the increase in zirconium content.

**3.6. Photocatalytic Activities.** Photocatalytic activities of the resulting solid solutions were investigated on the degradation of rhodamine B in aqueous solution. The red color of the solution gradually diminished upon the simulated solar light irradiation in the presence of photocatalysts, illustrating the degradation of RhB. Total concentrations of all rhodamine species were simply determined by the maximum absorption measurement. Figure 6 shows the decrease of the concentration of RhB virus irradiation time in the presence of the as-prepared $Ti_{1-x}Zr_xO_2$ samples and P25 as well as self-degradation of RhB under simulated solar light irradiation. It was found that the self-degradation of RhB was negligible under our simulated solar light irradiation. However, the degradation of RhB became obvious in the presence of photocatalysts. After 4 h of light irradiation, 36.6% RhB was photodegraded by P25, while degraded RhB in the presence of the $Ti_{1-x}Zr_xO_2$ solid solutions were 36.1%, 68.3%, 40.3%, and 26.8% for $x$ equaled to 0.045, 0.090, 0.135, and 0.180, respectively. These values were higher than degradation rate of 26% for pure $TiO_2$ without zirconium substitution ($x = 0.000$). Therefore, with the increase of zirconium content, the photocatalytic activities of $Ti_{1-x}Zr_xO_2$ solid solutions first increased and then decreased. This is consistent with the previous result.[23] The $Ti_{0.91}Zr_{0.09}O_2$ solid solution possessed the highest photocatalytic activity. Its activity was much higher than that of P25.

According to Yu and co-workers, the enhancement on the photocalatic activities of $Ti_{1-x}Zr_xO_2$ solid solutions by zirconium substitution was attributed to the presence of an additional pathway for the generation of hydroxyl radicals and the highly reactive atomic oxygen species. They proposed photocatalytic reactions on $Ti_{1-x}Zr_xO_2$ solid solutions as follows:[23]

$$Ti_{1-x}Zr_xO_2 + h\nu \leftrightarrow h^+ + e^- \quad (1)$$

$$OH^-(ads) + h^+ \rightarrow OH^\bullet \quad (2)$$

$$O_2(ads) + e^- \rightarrow O_2^-(ads) \quad (3)$$

$$O^{2-}(L) + h^+ \rightarrow O^- \quad (4)$$

$$O^- + h^+ \rightarrow O \quad (5)$$

$$O^-(ads) + h^+ \rightarrow O \quad (6)$$

$$O^- (O^-(ads)) + H_2O(ads) \rightarrow OH^\bullet(ads) + OH^-(ads) \quad (7)$$

Here the symbol "ads" denotes a species adsorbed on the surface of a catalyst and $O^{2-}(L)$ represents the oxygen species that escape from the surface of the lattice.

Yu and co-workers thought that pure $TiO_2$ photocatalyst with fewer defects would not have reactions 4−7 in the above photocatalytic mechanisms. So they further concluded that the lattice $O^{2-}$ and $O^-$ ionosorbed on surface were responsible for the increased photoactivity of solid solutions.[23]

In our study, the enhancement on photocatalytic activity of $TiO_2$ through the formation of $Ti_{1-x}Zr_xO_2$ solid solutions can also be attributed to the above reasons. That is, the substitution of zirconium would result in the lattice $O^{2-}$ and $O^-$ ionosorbed on surface, which could enhance the photocatalytic activity of solid solution photocatalysts. Besides these reasons, we believe the enlargement of band gap by zirconium substitution may also be helpful for the enhancement of photocatalytic activities of solid solutions because a larger band gap corresponds to a more powerful redox ability.[41] We thought that the crystal sizes of solid solutions did not influence the photocatalytic activity much because zirconium substitution did not significantly change the crystal sizes. Obviously, the substitution of zirconium enlarged the surface areas of photocatalytsts, which also accounts for the enhancement of solid solution photocatalysts. The relatively poor photocatalytic activities of the solid solution with higher zirconium contents ($x = 0.135$ and 0.180) was thought to be the reason for the existence of excess $ZrO_2$ arising from the nonincorporated zirconium in the solid solutions.[23] We used X-ray photoelectron spectroscopy to determine the amount of $ZrO_2$ in the resultants. According to XPS measurements on $Ti_{0.91}Zr_{0.09}O_2$ solid solution (Supporting Information), it can be found that the peaks for Zr $3d_{5/2}$ are composed of two signals. On the basis of the peak area ratio of the two signals, the ratio of Zr in the form of $ZrO_2$ in $Ti_{0.91}Zr_{0.09}O_2$ solid solution is about

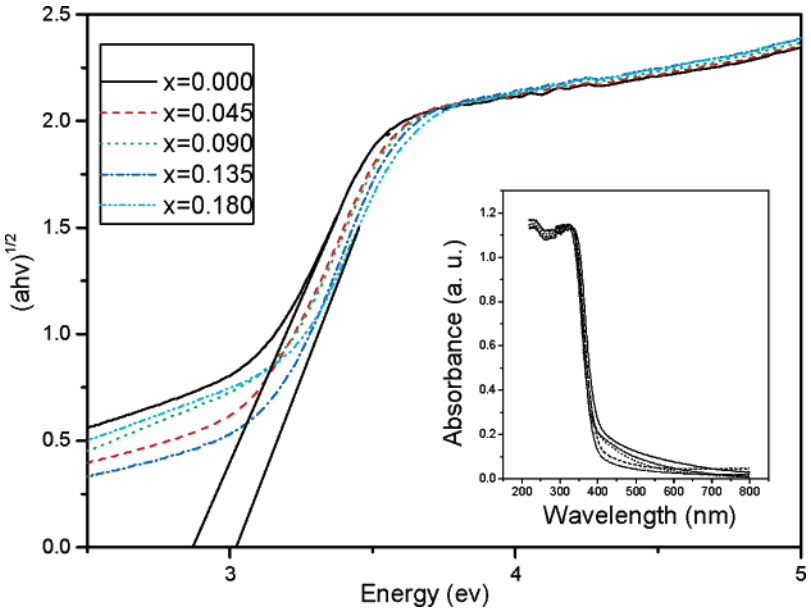


**Figure 4.** Plots of the $(ahv)^{1/2}$ versus the energy of absorbed light of the as-prepared $Ti_{1-x}Zr_xO_2$ samples ($x$ = 0.000, 0.045, 0.090, 0.135, and 0.180) and UV−vis diffuse reflectance spectra (inset).

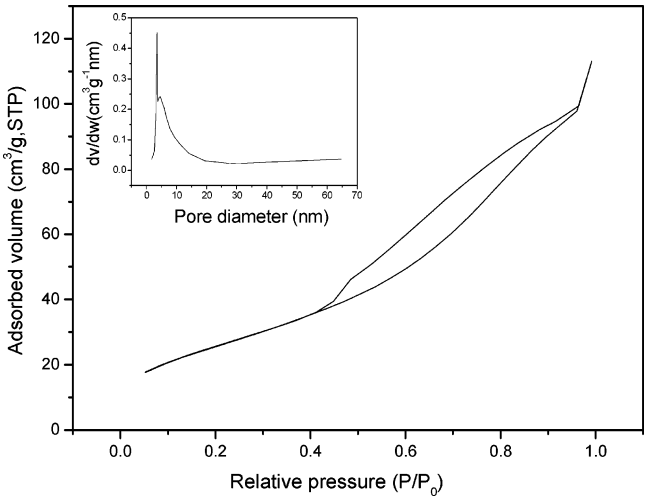


**Figure 5.** Representative nitrogen adsorption−desorption isotherm and pore size distribution curve (inset) of $Ti_{0.72}Zr_{0.18}O_2$ solid solution.

**TABLE 1: Textural Properties of the As-Prepared $Ti_{1-x}Zr_xO_2$ Samples ($x$ = 0.000, 0.045, 0.09, 0.135, and 0.180)**

| $x$ in $Ti_{1-x}Zr_xO_2$ | $A_{BET}$ ($m^2$/g) | $V_{BJH}$ ($cm^3$/g) | pore diameter (nm) |
|---|---|---|---|
| 0.000 | 39.3 | 0.23 | 3.68 |
| 0.045 | 52.9 | 0.28 | 3.31 |
| 0.090 | 67.9 | 0.28 | 3.37 |
| 0.135 | 77.0 | 0.27 | 3.42 |
| 0.180 | 96.4 | 0.45 | 0.45 |

43%. We believe that the contents of unsubstituted $Zr^{4+}$ ions in the form of $ZrO_2$ in solid solutions with higher zirconium contents ($x$ = 0.135 and 0.180) should be more than 43%. It is known that the band gap energy of $ZrO_2$ (~5 eV) is much higher than that of anatase $TiO_2$ (3.2 eV). Therefore, the presence of $ZrO_2$ in a solid solution could decrease its photocatalytic activity because $ZrO_2$ is difficult to be excited even by UV light. Meanwhile, the excess amounts of $ZrO_2$ in the sample may shield the photocatalyst from UV light, resulting in a poor activity.

**3.7. Formation of Core−Shell Structured Solid Solution Spheres.** We propose a possible formation mechanism for the core−shell-structured $Ti_{1-x}Zr_xO_2$ solid solution spheres as follows. It is widely believed that the droplets, when sprayed into a tubular reactor under pyrolysis conditions, serve as microreactors and yield one particle/droplet.[34] Meanwhile, larger droplets may contain several sub-microreactors. When the reaction takes place in the furnace tube at high temperature, the structures of big hollow spheres (shell) enwrapped with small spheres (core) would form after solvent evaporation (Figure 2e). Meanwhile, the inward heat transfer in microspheres would result in faster crystal growth of particles on sphere surfaces than those in the inner parts of spheres. This difference of crystal growth leads to the formation of a smooth surface (shell) and rough inner (core) as shown in Figure 2b. We think the formation mechanism of these core−shell $Ti_{1-x}Zr_xO_2$ solid solution spheres is different from that of anatase−rutile core−shell-structured titania particles through partial phase transformation of anatase to rutile by thermal treatment at 800 °C, where the mechanism of core−shell structure formation was proposed as the shrinkage during anatase to rutile phase transformation, the difference in the thermal expansion coefficient (TEC) of two crystals, and further decomposition of remaining organic

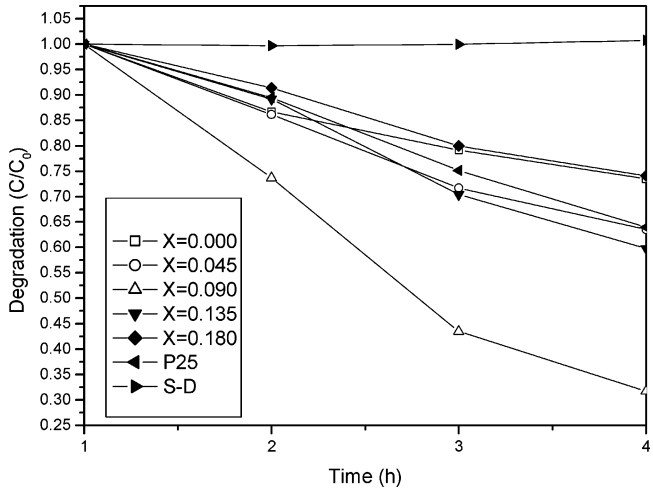


**Figure 6.** Comparison of the photocatalytic degradation of RhB in the presence of P25, $Ti_{1-x}Zr_xO_2$ ($x$ = 0.000, 0.045, 0.09, 0.135, and 0.180), and self-degradation (S-D) under simulated solar light irradiation.

components trapped in the core.[42] When $Zr^{4+}$ (with an ionic radius of 0.72 Å) substituted $Ti^{4+}$ (with an ionic radius of 0.605 Å) in the $TiO_2$ lattice to form $Ti_{1-x}Zr_xO_2$, the solid solution existed in a strained form with high lattice energy. Different substitution means different lattice energy. This may explain why the structures of the solid solutions change as the concentration of zirconium changes.

## 4. Conclusion

In summary, a series of $Ti_{1-x}Zr_xO_2$ solid solutions was obtained directly by an ultrasonic spray pyrolysis method in 1 h. The resulting solid solutions were of core−shell spherical structures. All the as-prepared solid solutions showed higher photocatalytic activities than pure $TiO_2$ without zirconium substitution. The $Ti_{0.91}Zr_{0.09}O_2$ solid solution showed the highest photocatalytic activity. Its activity was much higher than that of P25. Moreover, we successfully extended our method to prepare spherical $Ce_{1-x}Zr_xO_2$ solid solutions, indicating its generality (Supporting Information). Because of easily available equipment and inexpensive starting chemicals as well as time saving, we think our method may be easily scaled up for industrial production of spherical solid-solution photocatalysts for environmental applications and spherical catalysts for three-way catalytic (TWC) converters.

**Acknowledgment.** The work described in this paper was partially supported by the National Science Foundation of China (Grants 20503009, 20373025, and 20528302), Open Funds of Key Laboratory of Catalysis and Materials Science of Hubei Province (Grants CHCL0508 and CHCL06012), Jiangsu Provincial Natural Science Foundation of China (Grants BK2006718 and BK2006127), and Jiangsu Provincial High Technology Research Project (Grant BG2006030). Zhigang Zou thanks the Talent Project of Jiangsu Province.

**Supporting Information Available:** Nitrogen adsorption−desorption isotherms and pore size distribution curves of the $Ti_{1-x}Zr_xO_2$ solid solutions, a high-resolution XPS spectrum of Zr in $Ti_{0.91}Zr_{0.09}O_2$ solid solution, the synthesis procedure, XRD patterns, and SEM images of $Ce_{1-x}Zr_xO_2$ solid solutions. The material is available free of charge via the Internet at http://pubs.acs.org.

## References and Notes

(1) Ollis, D. F.; Al-Ekabi, H. *Photocatalytic Purification and Treatment of Water and Air*; Elsevier: Amsterdam, 1993.
(2) Fox, M. A.; Dulay, M. T. *Chem. Rev.* **1993**, *93*, 341.
(3) Linsebigler, A. L.; Lu, G. Q.; Yates, J. T. *Chem. Rev.* **1995**, *95*, 735.
(4) Hoffmann, M. R.; Martin, S. T.; Choi, W. Y.; Bahnemann, D. W. *Chem. Rev.* **1995**, *95*, 69.
(5) Ollis, D. F.; Pelizzetti, E.; Serpone, N. *Environ. Sci. Technol.* **1991**, *25*, 1522.
(6) Vogel, R.; Meredith, P.; Kartini, I.; Harvey, M.; Riches, J. D.; Bishop, A.; Heckenberg, N.; Trau, M.; Rubinsztein-Dunlop, H. *ChemPhysChem* **2003**, *4*, 595.
(7) Frach, P.; Gloss, D.; Goedicke, K.; Fahland, M.; Gnehr, W. M. *Thin Solid Films* **2003**, *445*, 251.
(8) Du, X. Y.; Wang, Y.; Mu, Y. Y.; Gui, L. L. Wang, P.; Tang, Y. Q. *Chem. Mater.* **2002**, *14*, 3953.
(9) Hansel, H.; Zettl, H.; Krausch, G.; Kisselev, R.; Thelakkat, M.; Schmidt, H. W. *Adv. Mater.* **2003**, *15*, 2056.
(10) Kron, G.; Rau, U.; Werner, J. H. *J. Phys. Chem. B* **2003**, *107*, 13258.
(11) Bosc, F.; Ayral, A.; Albouy, P. A.; Guizard, C. *Chem. Mater.* **2003**, *15*, 2463.
(12) Nakamura, R.; Imanishi, A.; Murakoshi, K.; Nakato, Y. *J. Am. Chem. Soc.* **2003**, *125*, 7443.
(13) Sung, Y. M.; Lee, J. K. *Cryst. Growth Des.* **2004**, *4*, 737.
(14) Shin, Y.-K.; Chae, W.-S.; Song, Y. M.; Sung, Y.-M. *Electrochem. Commun.* **2006**, *8*, 465.
(15) Lin, Y. M.; Tseng, Y. H.; Huang, J. H.; Chao, C. C.; Chen, C. C.; Wang, I. *Environ. Sci. Technol.* **2006**, *40*, 1616.
(16) Asahi, R.; Morikawa, T.; Ohwaki, T.; Aoki, K.; Taga, Y. *Science* **2001**, *293*, 269.
(17) Khan, S. U. M.; Al-Shahry, M.; Ingler W. B. *Science* **2002**, *297*, 2243.
(18) Sakthivel, S.; Kisch, H. *Angew. Chem., Int. Ed.* **2003**, *42*, 4908.
(19) Burda, C.; Lou, Y. B.; Chen, X. B.; Samia, A. C. S.; Stout, J.; Gole, J. L. *Nano Lett.* **2003**, *3*, 1049.
(20) Irie, H.; Watanabe, Y.; Hashimoto, K. *J. Phys. Chem. B* **2003**, *107*, 5483.
(21) Gole, J. L.; Stout, J. D.; Burda, C.; Lou, Y. B.; Chen, X. B. *J. Phys. Chem. B* **2004**, *108*, 1230.
(22) Yu, J. C.; Lin, J.; Kwork, R. W. M. *J. Photochem. Photobiol., A* **1997**, *111*, 199.
(23) Yu, J. C.; Lin, J.; Kwork, R. W. M. *J. Phys. Chem. B* **1998**, *102*, 5094.
(24) Yu, J. C.; Zhang, L. Z.; Lin, J. *J.Colloid. Interface Sci.* **2003**, *260*, 240.
(25) Oliveira, M. M.; Schnitzler, D. C.; Zarbin, A. J. G. *Chem. Mater.* **2003**, *15*, 1903.
(26) Cao, Y.; Zhou, Y. M.; Shan, Y.; Ju, H. X.; Xue, X. J.; Wu, Z. H. *Adv. Mater.* **2004**, *16*, 1189.
(27) Lin, J.; Yu, J. C.; Lo, D.; Lam, S. K. *J. Catal.* **1999**, *183*, 368.
(28) Tsuji, I.; Kato, H.; Kudo, A. *Angew. Chem., Int. Ed.* **2005**, *44*, 3568.
(29) Maeda, K.; Takata, T.; Hara, M.; Saito, N.; Inoue, Y.; Kobayashi, H.; Domen, K. *J. Am. Chem. Soc.* **2005**, *127*, 8286.
(30) Kudo, A.; Tsuji, I.; Kato, H. *Chem. Commun.* **2002**, 1958.
(31) Lu, Y. F.; Fan, H. Y.; Stump, A.; Ward, T. L.; Rieker, T.; Brinker, C. J. *Nature* **1999**, *398*, 223.
(32) Skrabalak, S. E.; Suslick, K. S. *J. Am. Chem. Soc.* **2005**, *127*, 9990.
(33) Jiang, X. M.; Brinker, C. J. *J. Am. Chem. Soc.* **2006**, *128*, 4512.
(34) Messing, G. L.; Zhang, S. C.; Jayanthi, G. V. *J. Am. Ceram. Soc.* **1993**, *76*, 2707.
(35) Gandhi, A. S.; Jayaram, V.; Chokshi, A. H. *Mater. Sci. Eng., A* **2001**, *304*, 785.
(36) Zhang, S. C.; Messing, G. L.; Huebner,W. *J. Aerosol Sci.* **1991**, *22*, 585.
(37) Lim, M. A.; Kang, Y. C.; Park, H. D. *J. Electrochem. Soc.* **2001**, *148*, H171.
(38) Suh, W. H.; Suslick, K. S. *J. Am. Chem. Soc.* **2005**, *127*, 12007.
(39) Didenko, Y. T.; Suslick, K. S. *J. Am. Chem. Soc.* **2005**, *127*, 12196.
(40) Sing, K. S. W.; Everett, D. H.; Haul, R. A. W.; Moscou, L.; Pierotti, R. A.; Rouquerol, J.; Siemieniewska, T. *Pure Appl. Chem.* **1985**, *57*, 603.
(41) Yu, J. C.; Zhang, L. Z.; Yu, J. G. *Chem. Mater.* **2002**, *14*, 4647.
(42) Sung, Y.-M.; Lee, J.-K.; Chae, W.-S. *Cryst. Growth Des.* **2006**, *6*, 805.